SUPPLEMENTAL MATERIAL

Experimental setup: The liquid viscosity was varied in our experiments by using glycerin/water mixtures of various mass fractions, 0, 40, 50, 60, 65, 70, 75, and 80% of glycerin. The impact velocity was changed by releasing the drops from between 0.16-2.16 m height. By varying the circular steel nozzle size, we used four different drop diameters: 3.2, 4.6, 5.1, and 5.7 mm. Further imaging details of the experiments can be found in Thoroddsen et al. [6].

Numerical simulations: We are using the GERRIS code [19] to solve the incompressible Navier-Stokes equations with the *Volume-Of-Fluid* method. Direct comparison between the experimental observations and numerical results were done over a set of different impact conditions. The same parameters as in the experiments were used for the numerical simulations. The air has a density of 1.21 kg/m^3, and a viscosity of 1.81×10^{-2} cP. Surface tension was kept constant, at 67.4 mN/m, neglecting the small variations with water/glycerin mixture fraction. Gravity was also taken into account with $g = 9.81$ m/s^2, and the drop diameter was kept constant $D = 4.6$ mm. The Re and K parameters were varied by changing the liquid viscosity, and impact velocity, in a similar way as in the experiments. Contrary to previous studies [8, 14, 15], the air cushioning effect is not neglected. The simulation starts before contact between the drop and the pool (Fig. S1), capturing the air disk trapped below the drop [Figs. S3(d), 4(a), and 4(d)]. The importance of the air properties on splashing has been highlighted by recent studies on drop impact on a solid surface [20–25].

A convergence study of a bumping case showed that a minimum cell size about 1000 times smaller than the drop diameter was necessary to observe the bumping shapes, explaining why previous studies could not capture this evolution. However, a much finer grid is needed to reproduce the evolution of very thin ejecta sheets occurring at the highest Re. This was accomplished using up to 16 levels of grid refinement, which means separating the domain locally into two smaller cells 16 times in each direction (the size of the smallest cell is 2^{16} times smaller than the domain). In our simulations, this corresponds to 28,800 cells per drop diameter. At this level of refinement, an equivalent uniform grid would have more than 4 billion cells $[(2^{16})^2]$, while our simulation have of the order of 20 million cells.

The minimum level of refinement in the domain was kept at 9, equivalent to a uniform grid of 512x512 cells. The grid was then refined dynamically based on vorticity and interface conditions. The grid was also kept uniform inside the ejecta sheet at the maximum level of refinement [Fig. S2(c)]. At the highest level of refinement, the ejecta sheet can become as thin as 500 nm (only 3 cells) near the tip, due to the extreme stretching. This value is consistent with our earlier indirect experimental measurements [6]. The results in the main text are at level 14, calculated on 64 processors, thereby allowing a systematic investigation of the parameter space.

The curvature of the tracer isolines was estimated by fitting a Bézier curve of order 3 through 5 points. For

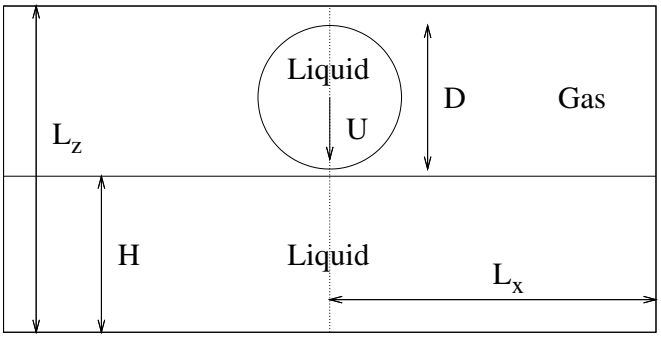

FIG. S1. Initial conditions in the GERRIS simulations. The domain of computation is limited to the right half of the domain drawn above, due to the axisymmetry. The proportions are reproduced here as in the simulations: $D = 0.44$, $H = 0.48$, $L_x = L_z = 1$, and the initial gap between the drop and the pool is 0.022, i.e., 10% of the drop radius.

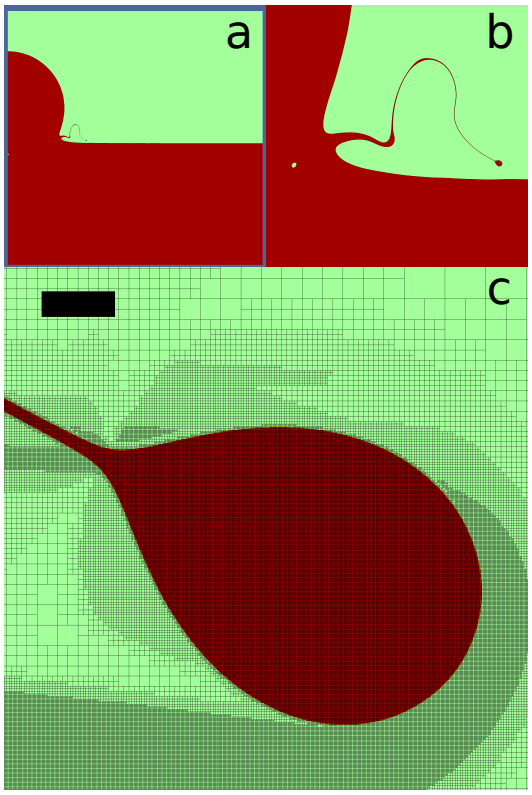

FIG. S2. (a) Overall simulation domain. (b) Zoom on the ejecta shape. (c) Typical grid near the tip of the ejecta sheet at a level 16 of refinement. The scale bar is $2 \times 10^{-3} D$ long.

smaller curvature cases, the number of points was increased to 11, improving the estimate of the position of maximum curvature.

Onset of Vortex Shedding: An intriguing question remains, i.e., what causes the oscillations of the ejecta base? Figure S3 shows our attempt to answer this. At a lower Reynolds number than the one showed in Fig. 4(c), small oscillations can be identified in the early evolution of the ejecta sheet [Fig. S3(a)]. They are visible also in the early times of Figs. 3(c) and 3(d), with less details. However, they stop rapidly, and do not lead to the breakup of the ejecta sheet [Figs. S3(b) and S3(d)]. We conclude that vorticity layers can be shed, but as soon as these layers start to break up into isolated vortices the base of the ejecta starts to oscillate. However, the transition onset to shedding is gradual, and the first oscillations at the base are not sufficiently strong to break up the jet, but rather make it wiggle, leaving slight bends in its shape [see Fig. S3(b)]. The analogy for vortex shedding behind solid cylinders, is the formation of symmetric separation bubble, which subsequently at some critical *Re* starts oscillating sideways starting the vortex shedding. The strong sideways forces due to this shedding can then feed back to the solid structure, through aeroelastic effects, making high-rise buildings sway from side to side.

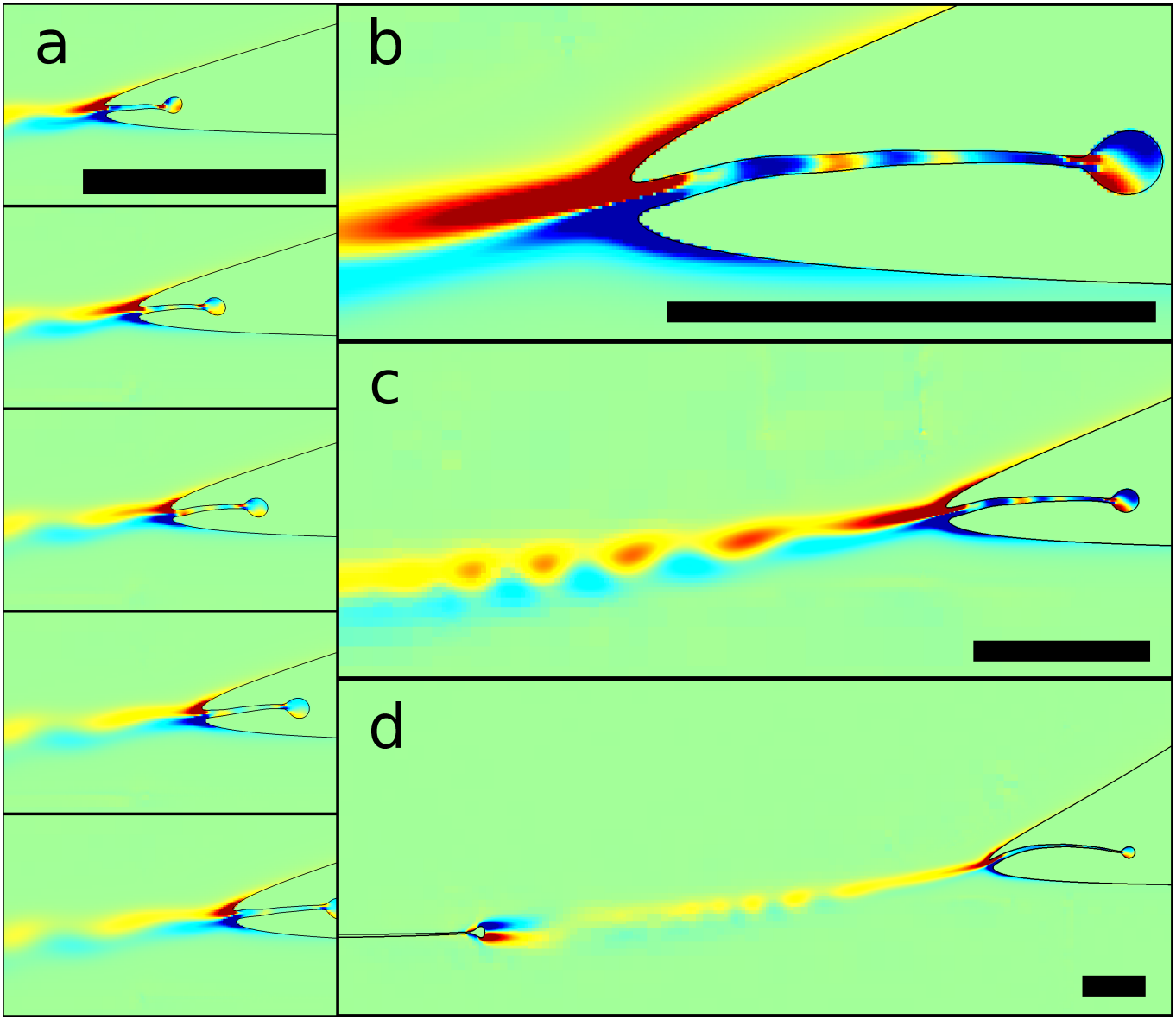

FIG. S3. Vorticity structures under the drop for $K = 7.44 \times 10^4$ and $Re = 6000$, i.e., slightly below the critical Reynolds number for irregular splashing. (a) Time sequence showing the small oscillations of the base of the ejecta sheet, at the same location as Fig. 4(g), starting at $t^* = 1.02 \times 10^{-2}$, and then with constant $\Delta t^* = 4.5 \times 10^{-4}$. The color scale is also kept identical to Fig. 4(g) to show the weaker levels of vorticity. (b) At a later time ($t^* = 1.82 \times 10^{-2}$), small oscillations are visible on the ejecta sheet, at the same locations as some vorticity shed from the base. (c) Larger view of (b), showing the first vorticity oscillations shed behind. The base of the ejecta sheet does not oscillate after this time. (d) Later evolution at $t^* = 2.95 \times 10^{-2}$. The first vortices shed are diffusing, and the ejecta sheet does not oscillate anymore. The thin line on the left corresponds to the air disk trapped below the drop, later contracting into a bubble [see also Fig. 4(d)]. The scale bars are all $0.02D$ long.